Frequency Doubling Conversion Efficiencies for Deep Space Optical Communications

D. L. Robinson and R. L. Shelton

Communications Systems Research Section

The theory of optical frequency doubling conversion efficiency is analyzed for the small signal input case along with the strong signal depleted input case. Angle phase matching and beam focus spot size are discussed and design trades are described which maximize conversion efficiency. Experimental conversion efficiencies from the literature, which are less than theoretical results at higher input intensities due to saturation, reconversion, and higher-order processes, are applied to a case study of an optical communications link from Saturn. Double pass conversion efficiencies as high as 45 percent are expected. It is believed that even higher conversion efficiencies can be obtained using multipass conversion.

I. Introduction

In a deep space optical communications link, a frequency doubled Nd:YAG laser transmitter emitting at 0.532 μm is the preferred transmitter. When the Nd:YAG laser is diode pumped the laser is completely solid state and has higher reliability for spacecraft communication than its gas and dye counterparts. The Nd:YAG laser fundamentally outputs at 1.06 μm. Since detectors typically have very low quantum efficiencies at 1.06 μm, the laser is frequency doubled to 0.532 μm to produce a wavelength that has higher detector quantum efficiencies. In this article, frequency doubling conversion efficiencies are discussed. First, in Section II, theoretical conversion efficiencies are discussed. Then, in Section III, experimental results from the literature are compared to the theoretical results presented in Section II. A case study is then presented that uses experimental data from the literature and typical optical communication link parameters for a link from Saturn. Finally, the conclusion is given in Section IV.

II. Theoretical Analysis

In 1961, second harmonic generation was first experimentally demonstrated with a conversion efficiency of approximately 10^{-8} [1]. Today conversion efficiencies of 30 to 40 percent are not uncommon. Second harmonic generation conversion efficiency for plane waves can be expressed as:

$$\eta = \frac{P(2\omega)}{P(\omega)} = 2\left(\frac{\mu_o}{\epsilon_o}\right)^{3/2} \frac{\omega^2 \, (d_{\text{eff}})^2 L^2}{n^3} \cdot \left(\frac{P(\omega)}{\pi \omega_o^2}\right) \frac{\sin^2\left(\frac{\Delta kL}{2}\right)}{\left(\frac{\Delta kL}{2}\right)^2} \quad (1)$$

for small input intensities (see Appendix A [2]). Here, $P(2\omega)/P(\omega)$ is the conversion efficiency, η, d_{eff} is the effective non-linear coefficient and ω is the fundamental frequency. The term $P(\omega)$ denotes the input power while $P(2\omega)$ denotes the second harmonic power. The variable L is the crystal length and Δk equals the difference between the wave vector $(k=2\pi/\lambda)$, k_2, for the second harmonic frequency, 2ω, and the wave vector k_1 for the fundamental frequency, ω. The beam waist radius is ω_0 and n is the index of refraction within the crystal. The quantities ϵ_0 and μ_0 are the electric and magnetic permeabilities, respectively, within a vacuum.

In Eq. (1), the $\sin^2 (\Delta kL/2)/(\Delta kL/2)^2$ factor can be made to approach unity, thus maximizing the conversion efficiency, with the proper phase matching techniques. Therefore, an understanding of phase matching is in order. If a second harmonic wave is produced at one plane and propagates to a second plane, and if another second harmonic wave is generated independently at this second plane, then the two waves interfere. The $\sin^2 (\Delta kL/2)/(\Delta kL/2)^2$ factor describes that interference, where $\Delta k = k_2 - 2k_1$. For maximum efficient frequency doubling, $\Delta k = 0$. Therefore, $k_2 = 2k_1$. A more detailed discussion of phase matching is given in Appendix B.

Looking at our initial conversion efficiency formula, Eq. (1), we have an inverse relationship between conversion efficiency and beam cross sectional area, $\omega_0^2 \pi$, assuming a uniform beam. This might lead one to tightly focus the beam. But because a tight focus results in greater divergence away from the beam waist, as Fig. 1 shows, minimizing the beam waist does not necessarily maximize the conversion efficiency. The confocal parameter, z, is defined as the distance from the plane of the beam waist to the plane in which the beam's cross sectional area is twice that at the beam waist (see Fig. 1).

$$z = \frac{\pi n \omega_0^2}{\lambda} \qquad (2)$$

It should be noted that some authors define the confocal parameter as twice that distance [3].

If the confocal parameter is much larger than the crystal length, then the beam's cross sectional area is relatively constant through the crystal. The plane wave formulation approximates this case. However, if the crystal length is much greater than $2z$, the decreased intensity away from the beam waist results in a lower overall conversion efficiency and a focused wave formulation must be used.

If $L=2z$, we have confocal focusing. By using $L=2z=2\pi n\omega_0^2/\lambda$, area $= \pi\omega_0^2$, and $\lambda = 2\pi c/\omega$ we obtain an equation for frequency doubling conversion efficiency for the focused case:

$$\frac{P(2\omega)}{P(\omega)}\bigg|_{\text{confocal focusing}} = \frac{2}{\pi c} \left(\frac{\mu_0}{\epsilon_0}\right)^{3/2} \frac{\omega^3 d^2 L}{n^2}$$

$$\times P(\omega) \frac{\sin^2\left(\frac{\Delta kL}{2}\right)}{\left(\frac{\Delta kL}{2}\right)^2} \qquad (3)$$

This formulation exhibits a conversion efficiency proportional to the crystal length, whereas in the plane wave model the conversion efficiency is proportional to L^2.

An exact analysis by Boyd and Kleinman [4] found that the conversion efficiency versus beam waist relationship follows the curve shown in Fig. 2. The optimum conversion results when $L = 5.68z$. This corresponds to an efficiency 20 percent greater than if $L = 2z$. Boyd and Kleinman's analysis incorporated an efficiency reduction factor in the conversion efficiency formula to analytically include the effect of focusing within the crystal. The efficiency reduction factor, h, is a function of crystal length, L, and the beam's confocal parameter, z. When $h(L/2z)$ enters the small input formula, Eq. (1), the yield is [4]:

$$\eta = 2\left(\frac{\mu_0}{\epsilon_0}\right)^{3/2} \frac{\omega^2 d_{\text{eff}}^2 L^2}{n^3} \left(\frac{P(\omega)}{\pi \omega_0^2}\right) h(L/2z) \qquad (4)$$

In Eq. 4 we assume complete phase matching ($\text{sinc}^2(\Delta kL/2) = 1$) and observe that the conversion efficiency is proportional to $h(L/2z)$. Therefore, conversion efficiency is maximized with the maximum h. Figure 2 illustrates the $h(L/2z)$ function versus $L/2z$. Here, and in Eq. (4), we have assumed the most efficient case where Boyd and Kleinman's double refraction parameter, which includes the effect of the walk-off angle between the Poynting vectors of the fundamental and the second harmonic waves [3], has been set to zero.

All the previous formulations required that conversion to the second harmonic be small. In other words, the amount of fundamental light traversing the crystal available for conversion to the second harmonic remained constant throughout the crystal. Since an optical communications application requires higher power levels with much greater conversion efficiencies, a discussion of the depleted input situation is warranted. In the depleted input case conversion efficiency is high; therefore, the amount of fundamental light traversing the crystal is continually reduced; hence, the term depleted input.

The equation for conversion efficiency for the depleted input case is given in Eq. (5) (see Appendix C):

$$\frac{P(2\omega)}{P(\omega)} = 2 \tanh^2 \left[d_{\text{eff}} \left(\frac{\mu_o}{\epsilon_o}\right)^{3/4} \frac{\omega z}{n^{3/2}} \sqrt{\frac{P(\omega)}{\pi \omega_o^2}} \right] \quad (5)$$

Single pass conversion efficiencies for the small signal input and depleted input formula are plotted in Fig. 3 for comparison. In Fig. 3, the upper curve is the small signal input formulation and the lower curve is the depleted input formulation for frequency doubling of 1064 nm radiation in a 5.1 mm KTP crystal. As can be seen from Fig. 3 the small signal formula is only valid for a small region, up to a conversion efficiency of approximately 15 percent. Beyond that region, the loss of input intensity due to conversion to the second harmonic is substantial and the small signal formula breaks down. The intensity of the beam decreases as the beam propagates through the crystal; thus, the conversion efficiency in the crystal decreases. Equation (5) assumes plane wave propagation within the crystal; however, the analysis by Boyd and Kleinman for focusing within the crystal could be applied to the depleted input case as well. Since an optical communication application requires high conversion efficiencies, the depleted input situation is appropriate.

III. Case Study

Let us examine a specific nonlinear frequency doubling crystal, $KTiOPO_4$ (KTP). The KTP crystal is a relatively new second harmonic generation material and has a few advantages over such predecessors as KDP and $LiNbO_3$. It has a high damage threshold and a high nonlinear coefficient, as well as excellent optical quality.

The d_{eff} values within the literature vary between theoretical and experimental results. By averaging the values of d_{eff}, which were determined from the graphical data presented in a Lockheed study of KTP [5], a value of 2.2×10^{-23} m/V was found. In Fig. 4 experimental values for single pass second-harmonic-generation conversion efficiency for a guassian beam have been graphed with theoretical values calculated in Section II for the depleted input case. At fundamental intensities less than 80 MW/cm² the two curves are in agreement. However, for intensities greater than 80 MW/cm² the experimental values are less than the expected theoretical results. Driscoll *et al.* attribute this saturation of reconversion to the fundamental and higher-order processes [5]. Driscoll *et al.* achieved higher conversion efficiencies with a multimode laser, probably due to localized higher intensity within the modal spot structure; however, for our application of deep space optical communication, we are primarily interested in single mode

TEM$_{oo}$ operation. Due to the difference in theory versus experiment, we use Driscoll's experimental data to calculate conversion efficiency in the following case study.

A specific case for frequency doubling is a cavity dumping scheme intended for an M-ary pulse position modulated (PPM) optical communications link [6]. As an example, assume a pulse repetition rate of 14.3 kHz (114 kbits/s for M=256) with a dead time of 44.4 μs and a pulse width of 20 ns. These parameters are typical of links being considered from Saturn to Earth. If an average laser power of 500 mW is assumed then the peak power is 1.75 kW with 35 μjoules as the corresponding pulse energy. An average spot diameter of 100 μm inside the crystal corresponds to a power density in the crystal of 22 MW/cm². Driscoll's graph of experimental data [5] for double pass efficiency through a 5.1 mm KTP crystal relates a 22 MW/cm² beam to approximately 28 percent double pass efficiency as shown in Fig. 5 with an arrow.

That conversion efficiency can be improved upon by decreasing the repetition rate, decreasing the average spot size, or increasing the average power level. Table 1 summarizes the results for various system parameters. Note that η in Table 1 only results from a double pass senario [5] and will probably be higher for multipass configurations.

A better understanding of the roles of spot size and pulse width can be gained by breaking down Table 1 and graphing the information. Figure 6 plots average power in watts versus double pass conversion efficiency for different spot sizes. Figure 6 shows that for the 50 μm beam, the conversion efficiency peaks and begins to drop off at approximately 500 mW, while the beam with a spot size of 100 μm peaks and begins to drop off at 2 watts. For two beams of the same average power, halving the spot diameter quadruples the intensity. At high intensities, the conversion efficiency decreases due to saturation, reconversion, higher order processes, and intensity fluctuations [5]. Thus, the curve for the 50 μm beam peaks and begins to dip at average power levels which are one fourth of those for similar efficiencies with a 100 μm beam. Figure 7 displays curves of double pass conversion efficiency versus average input power with a 10 ns pulse width and a 20 ns pulse width. For the specific case calculated, conversion efficiency peaks at 1.25 watts for the 10 ns pulse width case at a nominal pulse repetition rate of 14.3 kHz as discussed earlier. The 20 ns pulse width case peaks at a slightly higher average power level of 2.0 watts for the same repetition rate.

Furthermore, by varying the parameters, as the graphs and table display, double pass conversion efficiencies from 28 percent to 45 percent should be attainable for an optical communications link. However, even higher efficiencies are believed possible with a multipass system.

IV. Conclusion

A theoretical analysis of frequency doubling conversion efficiency has been presented along with a case study of an optical communications link from Saturn. The case study used experimental test results found in the literature and applied them to typical link parameters. An average power, 1 watt, laser operating at over 100 kbits/s in a pulse position modulation mode with M=256, and a pulse width of 10 ns, yielded double pass conversion efficiencies as high as 45 percent. Flux levels in this case, for a uniform average 100 μm diameter spot size, were approximately 90 MW/cm^2 which was well below the damage threshold of $\sim$350 MW/cm^2. Experimental conversion efficiencies found in the literature at this intensity level were in close agreement with those calculated from the theoretical discussion presented in Section I. At higher intensity levels, experimental results were less than those calculated due to saturation from reconversion and higher-order processes. With a multipass configuration, it is possible that still higher conversion efficiencies may be achievable.

References

[1] P. A. Franken, A. E. Hill, C. W. Peters, and G. Weinreich, "Generation of Optical Harmonics," *Phys. Rev. Letters*, vol. 7, pp. 118–119, 1961.

[2] A. Yariv. *Quantum Electronics*, New York: John Wiley and Sons, Inc., 1975.

[3] Y. R. Shen, *The Principles of Nonlinear Optics*, New York: John Wiley and Sons, Inc., 1984.

[4] G. D. Boyd and D. A. Kleinman, "Parametric Interaction of Focused Gaussian Light Beams," *Journal of Applied Physics*, vol. 39, no. 8, pp. 3597–3639, July 1968.

[5] T. A. Driscoll, H. J. Hoffman, R. E. Stone, and P. E. Perkins, "Efficient Second-Harmonic Generation in KTP Crystals," *J. Opt. Soc. Am. B*, vol. 3, no. 5, pp. 683–686, May 1986.

[6] D. L. Robinson, "A Novel Approach to a PPM Modulated Frequency Doubled Electro-Optic Cavity Dumped Nd:YAG Laser," to be published in JPL TDA Progress Report.

Table 1. Summary of various system parameters

| Spot diameter	Pulse width	Dead time	Rep rate M=256	Average power	Peak power	Power density	η
100 μm	20 ns	44.4 μs	14.3 kHz	500 mW	1.8 kW	22 MW/cm^2	28%
100 μm	20 ns	44.4 μs	14.3 kHz	1 W	3.5 kW	45 MW/cm^2	40%
100 μm	20 ns	44.4 μs	14.3 kHz	2 W	7.0 kW	89 MW/cm^2	45%
100 μm	20 ns	44.4 μs	14.3 kHz	3 W	10.5 kW	134 MW/cm^2	43%
50 μm	20 ns	44.4 μs	14.3 kHz	250 mW	0.88 kW	45 MW/cm^2	41%
50 μm	20 ns	44.4 μs	14.3 kHz	500 mW	1.8 kW	89 MW/cm^2	45%
50 μm	20 ns	44.4 μs	14.3 kHz	1 W	3.5 kW	179 MW/cm^2	43%
50 μm	20 ns	44.4 μs	14.3 kHz	2 W	7.0 kW	357 MW/cm^2*	40%
100 μm	10 ns	44.4 μs	14.3 kHz	500 mW	3.5 kW	45 MW/cm^2	40%
100 μm	10 ns	44.4 μs	14.3 kHz	1 W	7.0 kW	89 MW/cm^2	45%
100 μm	10 ns	44.4 μs	14.3 kHz	2 W	14.0 kW	178 MW/cm^2	43%

*damaged threshold
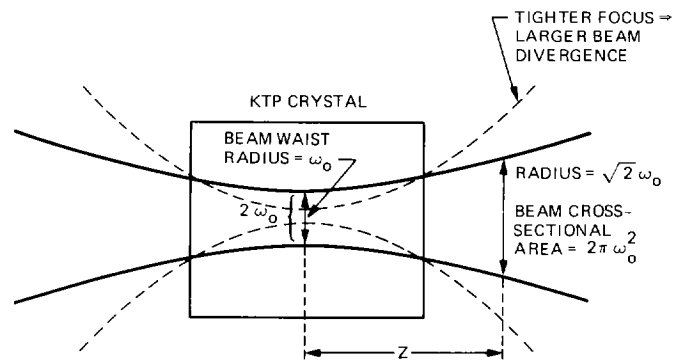
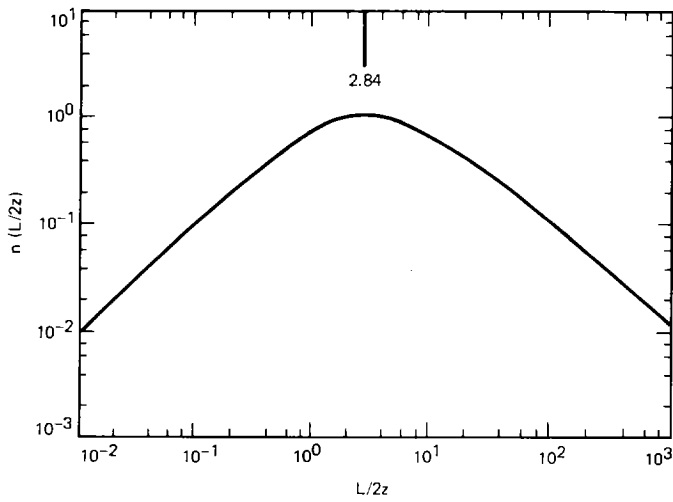**Fig. 1. Focusing of the beam through the frequency doubling crystal**

Fig. 2. Efficiency reduction factor, _h_, graphed as a function of _L/b_. Double refraction has been set to zero [4].
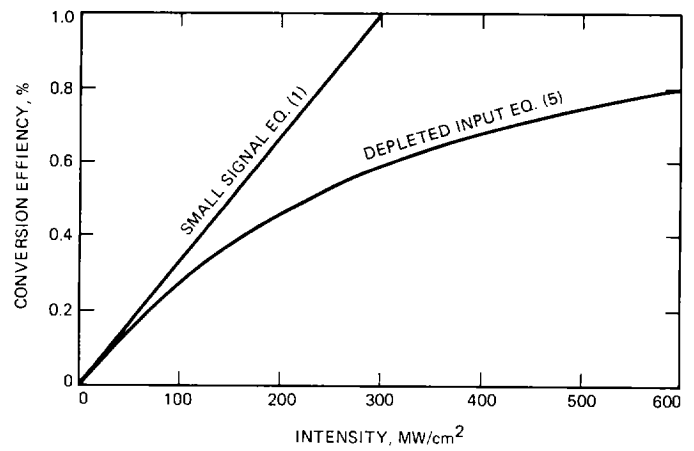

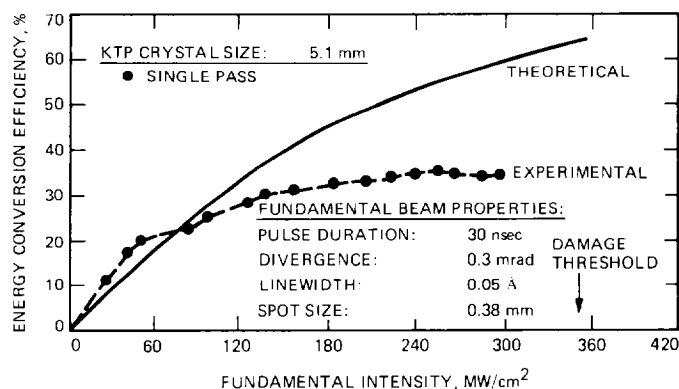**Fig. 3. Frequency doubling conversion efficiency has been graphed versus incident power density**

Fig. 4. Theoretical and experimental frequency doubling conversion efficiencies are plotted for single pass through a 5.1 mm KTP crystal. The saturation of the experimental results is due to reconversion and higher order processes.
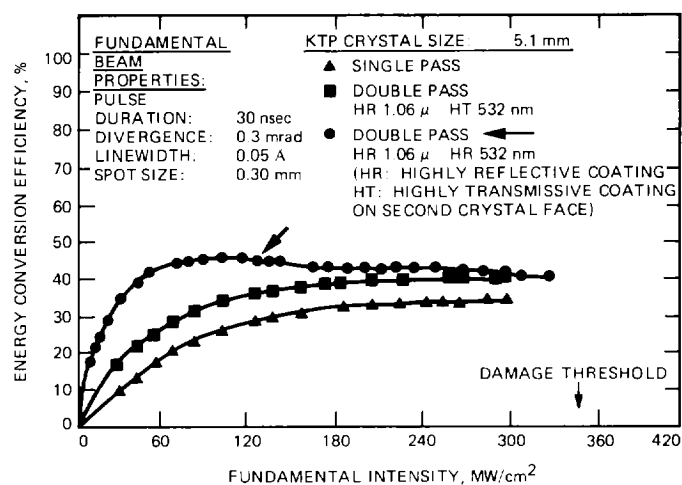
Fig. 5. Experimental conversion efficiency versus incident power density for a Gaussian 1.06 μm fundamental beam. The crystal was 5.1 mm in length [5].
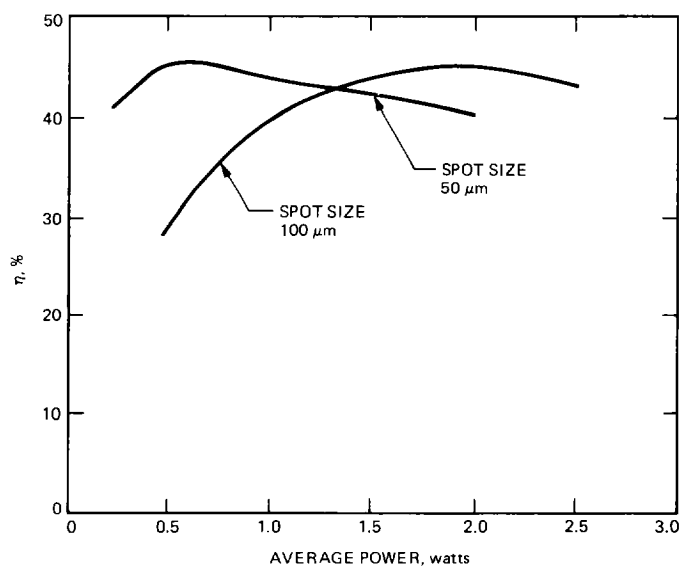
Fig. 6. Conversion efficiency versus average laser power for a PPM optical communications link. Assumed data rate is ~100 kbits with a pulse width of 20 ns and a dead time of 44.4 μs. Efficiencies for a 50 μm and 100 μm average spot size are graphed.
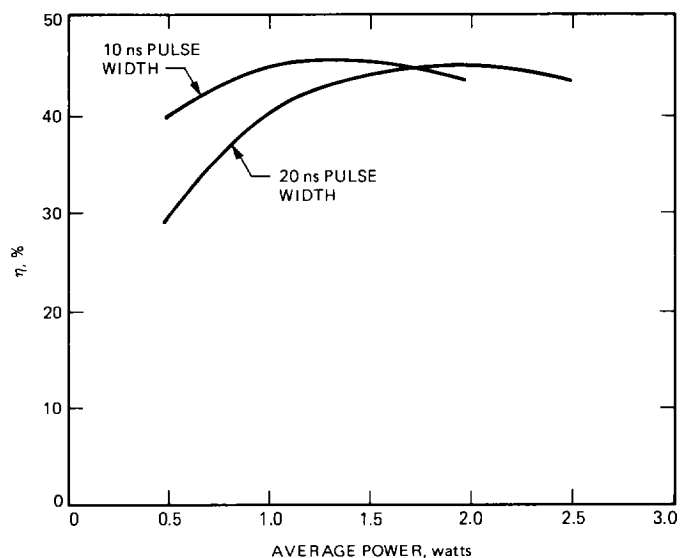
Fig. 7. Conversion efficiency versus average laser power for a PPM optical communications link. Assumed data rate is ~100 kbits with 44.4 μs dead time. Average spot size in the crystal was 100 μm. Efficiencies for pulse widths of 10 ns and 20 ns are graphed in the figure.

Appendix A
Conversion Efficiency

Crystals capable of higher order processes have nonlinear terms included in their polarization.

$$P = bE(1 + a_1E + a_2E^2 + a_3E^3 + \ldots)$$

where a_i and b are constants and E is the electric field. Specifically, let us examine the effect of the first nonlinearity, $P = dE^2$, which is responsible for second harmonic generation.

Starting with a one dimensional electric field traveling in the z direction, let us consider traveling waves of three frequencies, ω_1, ω_2, and ω_3.

$$E_1(\omega_1, z, t) = \frac{1}{2}[E_{1i}(z)\, e^{i(\omega_1 t - k_1 z)} + c.c.] \tag{A1}$$

$$E_k(\omega_2, z, t) = \frac{1}{2}[E_{2k}(z)\, e^{i(\omega_2 t - k_2 z)} + c.c.] \tag{A2}$$

$$E_j(\omega_3, z, t) = \frac{1}{2}[E_{3j}(z)\, e^{i(\omega_3 t - k_3 z)} + c.c.] \tag{A3}$$

Then, using the equation

$$\Delta^2 E = \mu_o \sigma \frac{\partial E}{\partial t} + \mu_o \epsilon \frac{\partial E^2}{\partial t^2} + \mu_o \frac{\partial^2 P_{NL}}{\partial t} \tag{A4}$$

where $(P_{NL})_i = d_{eff}E_j E_k$ is the nonlinear polarization and σ is the conductivity, it can be shown that

$$\frac{dE_{1i}}{dz} = \frac{-\sigma_1}{2}\sqrt{\frac{\mu_o}{\epsilon_1}}\, E_{1i}$$

$$-\frac{i\omega_1}{2}\sqrt{\frac{\mu_o}{\epsilon_1}}\, d_{eff} E_{3j} E_{2k}^* + e^{-i(k_3 - k_2 - k_1)z} \tag{A5}$$

$$\frac{dE_{2k}^*}{dz} = \frac{-\sigma_2}{2}\sqrt{\frac{\mu_o}{\epsilon_2}}\, E_{2k}^*$$

$$+\frac{i\omega_2}{2}\sqrt{\frac{\mu_o}{\epsilon_2}}\, d_{eff} E_{1i} E_{3j}^*\ e^{-i(k_1 - k_3 + k_2)z} \tag{A6}$$

$$\frac{dE_{3j}}{dz} = \frac{-\sigma_3}{2}\sqrt{\frac{\mu_o}{\epsilon_3}}\, E_{3j}$$

$$-\frac{i\omega_3}{2}\sqrt{\frac{\mu_o}{\epsilon_3}}\, d_{eff} E_{1i} E_{2k}\ e^{-i(k_1 + k_2 - k_3)z} \tag{A7}$$

For second harmonic generation, $\omega_1 = \omega_2$ and $\omega_3 = \omega_1 + \omega_2 = 2\omega_1$.

If we assume that the quantity of power lost by the input beam at ω_1 due to second harmonic conversion is negligible, then

$$\frac{dE_{1i}}{dz} \cong 0$$

As a result of the above two conditions only Eq. (A7) need be examined. Furthermore, the medium chosen will usually be transparent to radiation at ω_3, hence $\sigma_3 = 0$.

Therefore, Eq. (A7) reduces to the following:

$$\frac{dE_{3j}}{dz} = -i\omega\sqrt{\frac{\mu_o}{\epsilon}}\, d_{eff} E_{1i} E_{1k}\ e^{i\Delta k z} \tag{A8}$$

where

$$\Delta k = k_3 - k_1 - k_1$$

If we take $E_{3j}(0) = 0$ for no second harmonic input and let the frequency doubler's length be L, then the solution to Eq. (A8) is

$$E_{3j}(L) = -i\omega\sqrt{\frac{\mu_o}{\epsilon}}\, d_{eff} E_{1i} E_{1k}\ \frac{e^{i\Delta kL} - 1}{i\Delta k} \tag{A9}$$

where multiplication by E_{3j}^* leads to

$$E_{3j}(L)E_{3j}^*(L) = \frac{\mu_o}{\epsilon}\, \omega^2 d_{eff}^2$$

$$\times E_{1i}^2 E_{1k}^2 L^2\ \frac{\sin^2\left(\frac{\Delta kL}{2}\right)}{\left(\frac{\Delta kL}{2}\right)^2} \tag{A10}$$

This equation leads to an expression in terms of second harmonic output power when

$$\frac{P(2\omega)}{\text{Area}} = \frac{1}{2} \sqrt{\frac{\epsilon}{\mu_o}} \, E_{3j} E_{3j}^* \qquad \text{(A11)}$$

is substituted into it. Thus:

$$\frac{P(2\omega)}{\text{Area}} = \frac{1}{2} \sqrt{\frac{\mu_o}{\epsilon}} \, \omega^2 \, (d_{eff})^2 \, E_{1i}^2 E_{1k}^2 \, L^2 \, \frac{\sin^2\left(\frac{\Delta kL}{2}\right)}{\left(\frac{\Delta kL}{2}\right)^2}$$

$$\text{(A12)}$$

Utilizing a similar expression for $P(\omega)/\text{Area}$, an expression for conversion efficiency, $P(2\omega)/P(\omega)$ can be found to be:

$$\eta = \frac{P(2\omega)}{P(\omega)} = 2\left(\frac{\mu_o}{\epsilon_o}\right)^{3/2} \frac{\omega^2 \, d_{eff}^2 \, L^2}{n^3} \frac{P(\omega)}{\text{Area}} \frac{\sin^2\left(\frac{\Delta kL}{2}\right)}{\left(\frac{\Delta kL}{2}\right)^2}$$

$$\text{(A13)}$$

(note that $\epsilon = \epsilon_3$ and $\epsilon_1 \cong \epsilon_3 = \epsilon_o n^2$). See main text for definition of variables.

Appendix B

Crystal Angle Phase Matching

If the crystal is birefringent, having axially dependent indices of refraction, then $k(\omega) = \omega\,(\mu\epsilon_o)^{1/2}\,n(\omega)$. The k condition of $k_2 = 2k_1$, as discussed in the main text, translates to an $n(2\omega) = n(\omega)$ condition. Since in dispersive materials n is proportional to ω, it is not possible to match $n(2\omega)$ and $n(\omega)$ if the wave is propagating down a single crystal axis, because $n(2\omega)$ will always be larger. Therefore, in order to satisfy the equality of $n(\omega) = n(2\omega)$, a combination of the crystal indices of refraction is necessary. For uniaxial crystals, two axis indices are the same: $n_x = n_y = n_o$ and $n_z = n_e$ where z is the crystal optic axis, n_o is the ordinary index of refraction and n_e is the extraordinary index of refraction. Figure B1 is a graphical representation summarizing the indices of refraction for two orthogonal polarizations at varying angular propagation directions to the optic axis for differing wavelengths. In the graphs we are considering the case of the negative uniaxial crystal, $n_o > n_e$. The wave-vector, $\mathbf{D_o}$, propagates along s with an electric field polarized normal to the page. Thus, $\mathbf{D_o}$ remains constant, as seen by the circular representation of n_o, for varying propagation angles, θ. On the other hand, D_e has an electric field polarized perpendicular to $\mathbf{D_o}$ and the direction of propagation; thus, its magnitude varies for different propagation angles, θ. Figure B1(a) illustrates these index relationships at frequency ω while Fig. B1(b) illustrates them at 2ω. Note the increased size at 2ω due to the higher frequency. In order to obtain $n(\omega) = n(2\omega)$, the 2 curves are overlapped. The intersection of the two curves yields the desired answer. The solution results from using n_o at ω and $n_e(\theta)$ at 2ω as seen in Fig. B1(c). This angular solution is analytically described as follows:

$$\frac{1}{(n_e(2\omega,\theta))^2} = \frac{\cos^2\theta}{(n_o(\omega))^2} + \frac{\sin^2\theta}{(n_e(2\omega))^2} \tag{B1}$$

where θ is the angle between the ray's axis of propagation and the optic axis. This same type of analysis is used with biaxial crystals where $n_x \neq n_y \neq n_z$. Since all axes have different indices of refraction, the analysis is much more complicated.
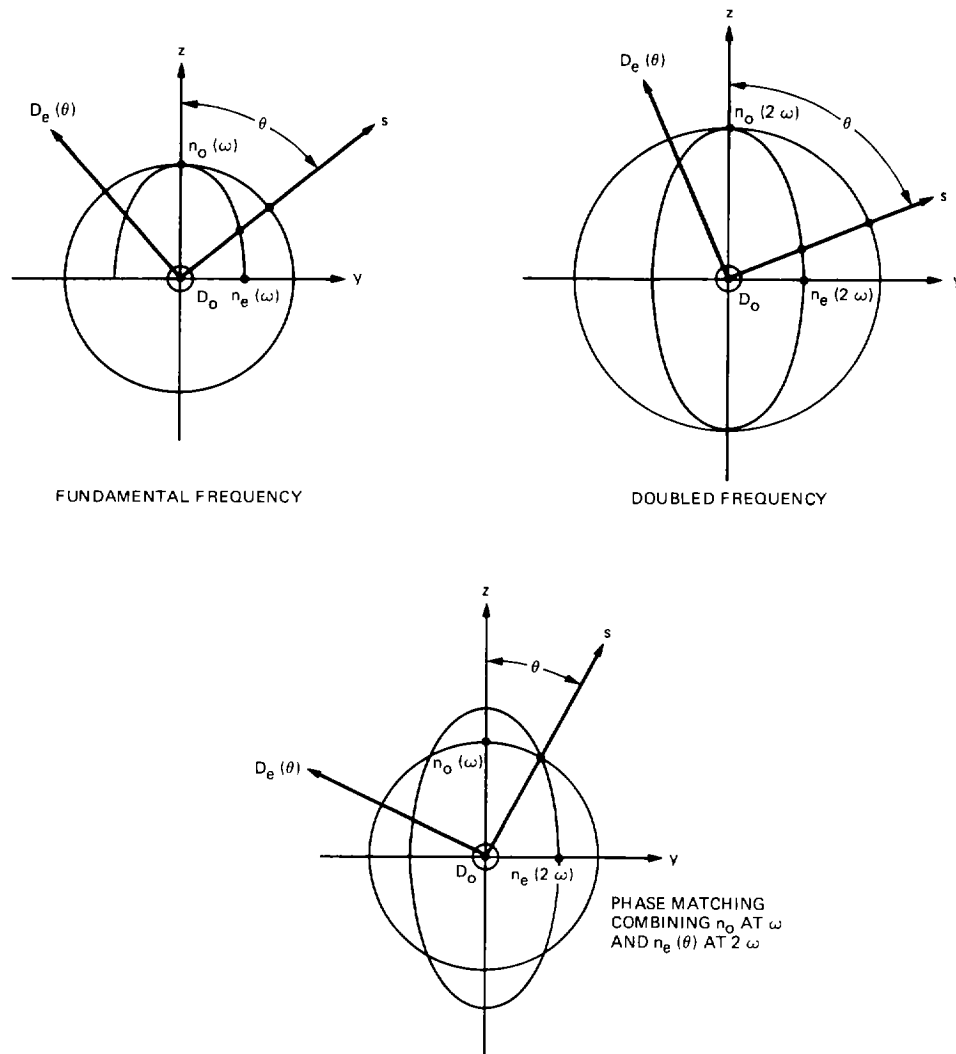
Fig. B1. Phase matching curves for ordinary and extraordinary indices of refraction

Appendix C

Depleted Input Conversion Efficiency

Let us utilize Eqs. (A5), (A6), and (A7) from Appendix A and follow a similar approach as found in Yariv [2].

$$\frac{dE_{1i}}{dz} = \frac{-\sigma_1(\mu_o)^{1/2}}{2(\epsilon_1)^{1/2}} E_{1i} - \frac{i\omega_1(\mu_o)^{1/2}}{2(\epsilon_1)^{1/2}} d_{eff} E_{3j} E_{2k}^* e^{-i\Delta kz}$$

(C1)

$$\frac{dE_{2k}^*}{dz} = \frac{-\sigma_2(\mu_o)^{1/2}}{2(\epsilon_2)^{1/2}} E_{2k}^* + \frac{i\omega_2(\mu_o)^{1/2}}{2(\epsilon_2)^{1/2}} d_{eff} E_{1i} E_{3j}^* e^{i\Delta kz}$$

(C2)

$$\frac{dE_{3j}}{dz} = \frac{-\sigma_3(\mu_o)^{1/2}}{2(\epsilon_3)^{1/2}} E_{3j} - \frac{i\omega_3(\mu_o)^{1/2}}{2(\epsilon_3)^{1/2}} d_{eff} E_{1i} E_{2k}^* e^{i\Delta kz}$$

(C3)

We can set $\sigma_1 = \sigma_2 = \sigma_3 = 0$ because the medium chosen should be transparent to radiation of the input frequency and the second harmonic. Furthermore, for frequency doubling, $E_1 = E_2$. Since the phases should be matched, $\Delta k = 0$. Also, if $E_1(0)$ is real, then $E_1(z)$ is real. Let us drop the $_{ijk}$ notation and define $E_3 = -iE_3'$.

Therefore, Eqs. (C1) and (C3) become:

$$\frac{dE_1}{dz} = \frac{-\omega_1 (\mu_o)^{1/2}}{2 (\epsilon_1)^{1/2}} d_{eff} E_3' E_1^*$$

(C4)

and

$$\frac{dE_3'}{dz} = \frac{\omega_3 (\mu_o)^{1/2}}{2 (\epsilon_3)^{1/2}} d_{eff} E_1^2$$

(C5)

Therefore,

$$\frac{d}{dz} E_1^2 + E_3'^2 \frac{\omega_1 (\epsilon_1)^{1/2}}{\omega_3 (\epsilon_3)^{1/2}} = 0$$

(C6)

If there is no input at ω_3, then integrating the above equation and substituting $\epsilon_o n^2 = \epsilon_1 \approx \epsilon_3$ yields:

$$E_1^2 + E_3'^2 \frac{(\omega_1)}{(\omega_3)} = E_1^2(0)$$

(C7)

Substituting E_1^2 into Eq. (C5) leads to:

$$\frac{dE_3'}{dz} = \frac{\omega_3(\mu_o)^{1/2}}{2(\epsilon_3)^{1/2}} d_{eff} \left(E_1^2(0) - \frac{\omega_1}{\omega_3} E_3'^2 \right)$$

(C8)

Integration of Eq. (C8) leads to:

$$E_3' = E_1(0) \left(\frac{\omega_3}{\omega_1} \right)^{1/2} \tanh \left(\frac{d_{eff} (\mu_o \omega_1 \omega_3)^{1/2} E_1(0) z}{2 (\epsilon_o n_1 n_3)^{1/2}} \right)$$

(C9)

Given that

$$\frac{P_1}{A} = \frac{n_1(\epsilon_o)^{1/2}}{2(\mu_o)^{1/2}} |E_1|^2$$

where A = beam area, and using $\omega_3 = 2\omega_1$, Eq. (C9) becomes:

$$\eta = \frac{P(2\omega)}{P(\omega)} = \frac{|E_3'|^2}{|E_1(0)|^2} = 2 \tanh^2 \left(\frac{d_{eff} (\mu_o)^{3/4} \omega_1 P_1^{1/2} z}{A^{1/2} \epsilon_o^{3/4} n^{3/2}} \right)$$

Making the small angle approximation leads to the small signal formula of Appendix A for conversion efficiency.